*J. Fluid Mech.* (1993), *vol.* 257, *pp.* 667–689



# Integral method for a two-dimensional Stokes flow with shrinking holes applied to viscous sintering

By G. A. L. VAN DE VORST

Department of Mathematics and Computing Science, University of Technology, P.O. Box 513, 5600 MB Eindhoven, The Netherlands

(Received 28 September 1992 and in revised form 21 June 1993)

An integral method is developed to solve the two-dimensional Stokes problem with Neumann boundary conditions for multiply connected domains in which the inside hole area can shrink and disappear. The method is applied to simulate viscous sintering. In particular the sintering of glasses can be modelled as such, i.e. a viscous incompressible Newtonian volume flow driven solely by surface tension. A Boundary Element Method is applied to solve the integral equations of Stokes flow involved, and the time integration is carried out by a variable-step, variable-order Backward Differences Formulae method. The derived numerical algorithm is demonstrated for several arbitrarily shaped multiply connected sintering domains. In particular some cylindrical packings are considered. The latter simulations provide a justification for the use of 'unit problems' in the theory of sintering.

## 1. Introduction

Sintering is the process of bringing a granular compact of metals, ionic crystals, or glasses to such a high temperature that sufficient mobility is present to release the excess free energy of the surface of the powder, thereby joining the particles together. For a survey of the most important papers on sintering we refer to the book edited by Sōmiya & Moriyoshi (1990).

In this paper, we consider the case of sintering glasses; here the material transport can be modelled as a viscous incompressible Newtonian volume flow, driven solely by surface tension (viscous sintering), i.e. the Stokes creeping flow equations hold. This sintering is in effect a three-dimensional problem. However, because of the complexity of such three-dimensional geometries, we restrict ourselves to simple shapes in two-dimensions only.

A large part of the theory of sintering that has been developed thus far can be brought back to the investigation of the behaviour of so-called 'unit problems'. Typical examples of such problems are the coalescence of two or an infinite line of both spheres and cylinders; these are the most simple unit problems. In the case of viscous sintering, more complicated unit problems have been developed, for example by Scherer (1984). These unit models are employed to describe the sintering of a complex structure like a glassy aerogel that can be used to produce a high-quality glass, cf. Kuiken (1990). Typically, a unit cell is determined in such an aerogel that represents the structure of the material considered. The sintering of this cell is

described by applying the unit problems. From the behaviour of this unit cell the properties of the sintering material considered are obtained.

Recently, Hopper (1990, 1992) solved analytically two unit viscous sintering problems, viz. the coalescence of two equal cylinders, cf. Hopper (1990), and the coalescence of a cylinder on a half-space, cf. Hopper (1992). He applied a conformal mapping technique to solve the Stokes equations in which the time evolution of the shape was described in terms of an equation of motion involving the mapping function. In Hopper (1990), the method is demonstrated for a number of regions which are bounded by a simple smooth closed curve. Hopper was also able to solve some problems for some semi-infinite regions. However, the examples in those papers show that his method depends on guessing a mapping function which initially has a built-in behaviour that describes the time evolution of the shape. The difficulty of finding such a mapping is illustrated in Hopper (1991): the only doubly connected domain he could solve was a circular disk with a circular hole centred at the origin. This problem can also be solved easily by describing the problem in cylindrical coordinates. Richardson (1992) was able to solve the unit problem of the coalescence of two unequal cylinders by applying Hopper's method.

The numerical simulation of the given initial geometry of a creeping Stokes flow is performed by successively solving the Stokes problem for that domain, and employing a time step to predict the next level geometry. The first simulation of a unit problem of viscous sintering was carried out by Ross, Miller & Weatherly (1981). They considered the sintering of an infinite line of cylinders and performed this simulation by employing a Finite Element Method (FEM) to solve the Stokes equations. Jagota & Dawson (1988*a*, 1990) also applied the FEM for two axisymmetric problems: the sintering of two spheres and an infinite line of spheres. In Jagota & Dawson (1988*b*) they used the behaviour of the two coalescing spheres, to describe the densification of a powder compact. In that model, the particle packing is modelled as a framework of links between the touching spheres and the development of those links is described by considering the behaviour of the two coalescing spheres separately.

Recently, Kuiken (1990) simulated viscous sintering problems for domains with moderately curved shapes; he used an integral representation in terms of the stream and vorticity function. A Boundary Element Method (BEM) was employed to solve the resulting equations. However, serious numerical problems occurred when simulating a geometry with a near cusp. Those problems were due to inaccuracies in computing the derivative of the curvature, which was required in that particular integral formulation.

In earlier work, (van de Vorst & Mattheij 1991, 1992*a*,*b*; van de Vorst, Mattheij & Kuiken 1992) we reported solutions of the problem for arbitrarily shaped simply connected fluid regions. These simulations were performed by solving the Stokes problem by applying a BEM to the integral formulation in terms of boundary distributions of hydrodynamical single- and double-layer potentials. After solving the Stokes equations, the time step is carried out by a more sophisticated time integrator: a variable-step, variable-order Backward Differences Formulae (BDF) scheme.

In all papers mentioned above, the simulation of viscous sintering problems was considered for simply connected domains only. In this paper, we consider the viscous sintering of two-dimensional arbitrarily shaped multiply connected domains. Therefore, we have to construct an integral formulation for this domain which has solutions with a certain type of singularity in order to model the shrinkage of holes inside the fluid.

A review of recent numerical techniques for the solution of Stokes flows is given by

Weinbaum, Ganatos & Yan (1990). Here only the evolution of the fluid boundary is required. Therefore the Stokes problem is reformulated by an integral equation based on hydrodynamic single- and double-layer potentials. Tanzosh, Manga & Stone (1992) gave a review of the numerical solution of free creeping Stokes flows whereby this type of integral formulation is applied. The books of both Kim & Karrila (1991) and Pozrikidis (1992) extensively outline the theoretical derivation and the practical application of such integral formulations for a wide range of physical problems.

Both of the latter books outline how the integral formulation for a simply connected domain can be extended to multiply connected domains. In order to derive a suitable solution from this integral, the equation has to be modified slightly. Besides rigid-body movements, which have to be prescribed also in the case of a simply connected domain, the boundary normal has to be prescribed too since it appears that this is an eigenfunction of the adjoint of the double-layer potential integral operator. In the above-mentioned books this is performed by deflation of the integral operator, i.e. the eigenvalues are removed. A more precise mathematical derivation of such an integral construction has been given by Hsiao & Kress (1985) for the case of an exterior two-dimensional Stokes problem. Kim & Karrila (1991) and Pozrikidis (1992) applied the method to a number of resistance and movement problems of solid and liquid particles in a Stokes flow. However in the case of viscous sintering, this method will not give the correct solution since we require that the holes can be filled up with fluid and vanish or that a hole can expand. Physically, this means that the porosity changes during sintering. Hence we have to model a *sink* inside those holes, cf. Batchelor (1967, p. 88). This sink contribution is formulated in a single integral equation which is applied as a constraint for the original equation and will be used to deflate that equation.

In §2 of this paper we briefly describe the viscous sintering model and give the integral representation for a simply connected domain. Furthermore, we outline the construction of the integral representation for a multiply connected domain. This integral equation will be solved by the BEM. Some important details about this solution will be briefly mentioned too. In §3.1 the numerical correctness of the algorithm will be shown by a simple test geometry, viz. the shrinkage of a circular disk with a circular hole centred at the origin, since this problem can be solved analytically. Then we show a number of examples to demonstrate the usefulness of our method. In particular we consider some cylindrical packings. The latter simulations will provide a justification for the use of 'unit problems' in the theory of sintering.

## 2. Problem description and solution

In this section we will briefly summarize the mathematical model that describes viscous sintering. Secondly, an integral formulation will be derived that is capable of representing the solution for a multiply-connected fluid domain with shrinking holes. Some remarks are made on the numerical solution of the problem thereafter.

### 2.1. *Problem description*

Viscous sintering can be modelled by the Stokes creeping flow equations, see also Kuiken (1990). These Stokes equations are basically governing the flow and read in dimensionless form

$$\nabla^2 \boldsymbol{v} - \nabla p = 0, \tag{2.1}$$

with the continuity equation

$$\nabla \cdot \boldsymbol{v} = 0. \tag{2.2}$$

Here $\boldsymbol{v}$ is the dimensionless velocity and $p$ the dimensionless pressure. The stress tensor $\boldsymbol{T}$ for a Newtonian fluid is defined by

$$T_{ij} = -p\delta_{ij} + \left(\frac{\partial v_i}{\partial x_j} + \frac{\partial v_j}{\partial x_i}\right). \tag{2.3}$$

In this paper, we apply the following (Neumann) boundary conditions which are valid in the case of viscous sintering, e.g. Kuiken (1990) and van de Vorst *et al.* (1992):

$$\boldsymbol{T}\boldsymbol{n} = \kappa \boldsymbol{n}, \tag{2.4}$$

where $\boldsymbol{n}$ is the outward unit normal vector of the boundary and $\kappa$ is the local boundary curvature. The boundary curvature is formulated as

$$\kappa = \nabla \cdot \boldsymbol{n}. \tag{2.5}$$

These equations can be solved uniquely for a *fixed* domain up to an arbitrary rigid-body translation and rotation, cf. van de Vorst *et al.* (1992). The displacement of the boundary is obtained by employing the boundary velocity solution $\boldsymbol{v}$ and the Lagrangian representation,

$$\frac{\mathrm{d}\boldsymbol{x}}{\mathrm{d}t} = \boldsymbol{v}(\boldsymbol{x}) \qquad (\boldsymbol{x} \in \Gamma), \tag{2.6}$$

where $t$ is the dimensionless time. This equation expresses the movement of the *material* particles, i.e. we are following the trajectories of those particles.

In the case of a multiply connected region, we assume that the normal component of the stress vector is proportional to the local curvature of the boundaries of the internal holes, cf. (2.4). Thus we exclude that the holes can move as a consequence of buoyancy or that there is an extra stress component due to a gas inside those holes. This is a reasonable simplification because in our problem formulation we did not include any gravity force since the sintering particles are very small. Hence the force due to gravity is neglected.

### 2.2. *Integral formulation*

From (2.6) it follows that we are interested only in the boundary velocity of the considered shape. Therefore this problem is ideally suited to being solved numerically by the BEM. To do this, we have to reformulate the problem as an integral equation over the boundary: we transform the Stokes equations with (Neumann) boundary conditions into an equivalent set of integral equations. We will start with the formulation for a simply connected domain and extend this equation to a multiply connected domain.

Consider a simply connected domain surrounded by a closed curve $\Gamma$ in the plane $\mathbb{R}^2$. For the two-dimensional Stokes problem, the following integral formulation can be deduced, cf. van de Vorst *et al.* (1992):

$$c_{ij}v_j + \int_\Gamma q_{ij}v_j \,\mathrm{d}\Gamma_y = \int_\Gamma \kappa u_{ij}n_j \,\mathrm{d}\Gamma_y. \tag{2.7}$$

Here $c_{ij}$, $q_{ij}$ and $u_{ij}$ are equal to respectively

$$\left.\begin{aligned} c_{ij} &= \begin{cases} \delta_{ij}, & x \text{ inside } \Gamma \\ \frac{1}{2}\delta_{ij}, & x \text{ on } \Gamma \\ 0, & x \text{ outside } \Gamma; \end{cases} \qquad q_{ij}(x,y) = \frac{r_i r_j}{\pi R^4} r_k n_k, \\ u_{ij}(x,y) &= \frac{1}{4\pi}\left[ -\delta_{ij} \log R + \frac{r_i r_j}{R^2} \right], \end{aligned}\right\} \tag{2.8}$$

where $r_i = x_i - y_i$, $R = (r_1^2 + r_2^2)^{\frac{1}{2}} = |x - y|$ and $\delta_{ij}$ is the *Kronecker delta.* Many authors attribute the above integral equation to Ladyzhenskaya (1963), but actually it was Lorentz who derived this formulation in essence, back in 1896. The integral on the left-hand side represents the double-layer potential and the single-layer potential is the other integral.

Equation (2.7) can not be solved uniquely since the homogeneous equation has three linearly independent solutions $\varphi^k$, i.e. the rigid-body motions

$$\varphi^k(x) = (\delta_{k1}, \delta_{k2})^{\mathrm{T}} \quad (k = 1,2) \qquad \text{and} \qquad \varphi^3(x) = (x_2, -x_1)^{\mathrm{T}}. \tag{2.9}$$

There are two main approaches to make (2.7) uniquely solvable. The first method is to add three additional variables that describe those rigid-body movements and, in order to achieve a full rank system, three integral constraints are included, cf. van de Vorst & Mattheij (1992*b*). The other method is to 'remove' the eigenvalue of the double-layer integral operator that causes this zero-space, i.e. $-\frac{1}{2}$, and construct a 'deflated' operator. This latter approach can be achieved by *Wielandt's deflation* which is extensively discussed in Kim & Karrila (1991) and Pozrikidis (1992). The advantage of deflation is that the number of unknowns does not change and that we do not have to seek extra integral constraints: it is a purely mathematical approach which will be applied in this paper too. Only the resulting integral formulation is summarized, for more details we refer to the above-mentioned references.

After 'deflating' (2.7), the following integral formulation is obtained for the simply connected domain:

$$c_{ij} v_j(x) + \int_\Gamma q_{ij}(x,y) v_j \, \mathrm{d}\Gamma_y + \varphi_i^k(x) \int_\Gamma \varphi_j^k v_j \, \mathrm{d}\Gamma = \int_\Gamma \kappa u_{ij}(x,y) n_j \, \mathrm{d}\Gamma_y. \tag{2.10}$$

The functions $\varphi^k$ are actually divided by the square root of the length of the boundary curve $\Gamma$ too. This is only for numerical reasons and therefore we will omit this in the integral formulations further on also. Now, there exists a unique solution $v$ of the above equation since the homogeneous part of (2.10) is bijective, cf. Kress (1989, p. 43). Moreover, the obtained solution $v$ also satisfies (2.7) because it can be shown that

$$\int_\Gamma \varphi_j^k v_j \, \mathrm{d}\Gamma = 0. \tag{2.11}$$

The next step will be the extension of the integral formulation to multiply connected domains. Let this domain be bounded externally by $\Gamma_0$ and internally by $\Gamma_1,..,\Gamma_M$. By $\Gamma$ we denote the complete boundary. If we formally apply the integral (2.7) to this multiply connected domain, we derive

$$c_{ij} v_j + \sum_{m=0}^{M} \int_{\Gamma_m} q_{ij} v_j \, \mathrm{d}\Gamma_y = \sum_{m=0}^{M} \int_{\Gamma_m} \kappa u_{ij} n_j \, \mathrm{d}\Gamma_y, \tag{2.12}$$

where the normal of the inner boundary is also pointing outward into the fluid.

Again, the rigid-body motion functions (2.9) are a basis for the zero-space of the homogeneous part of (2.12). Using those functions, the above double-layer potential can be deflated in a similar way as was done for the simply connected domain, cf. Kim & Karrila (1991).

Let $\varphi^{mk}(x)$ be the $k$th rigid-body movement of the hole enclosed by $\Gamma_m$ when $x \in \Gamma_m$, otherwise this function is taken equal to zero. The following deflated equation is obtained:

$$c_{ij}v_j(x) + \sum_{m=0}^{M} \int_{\Gamma_m} q_{ij}(x,y)v_j \,\mathrm{d}\Gamma_y + \varphi_i^{pk}(x) \int_{\Gamma_p} \varphi_j^{pk} v_j \,\mathrm{d}\Gamma = \sum_{m=0}^{M} \int_{\Gamma_m} \kappa u_{ij}(x,y)n_j \,\mathrm{d}\Gamma_y \quad (x \in \Gamma_p). \tag{2.13}$$

The integral formulation that has been derived so far cannot describe the shrinkage or the expansion of the inside holes of the fluid domain. This can be illustrated by the following example shape, viz. a circular fluid disk with a circular hole centred at the origin. This flow problem can be solved analytically, cf. §3.1, and one obtains that the interior hole of the annulus shrinks and vanishes as time increases. Physically, this means that the porosity decreases during sintering. However, when we put this particular shape into the integral formulation (2.13) the null solution is derived, since the right-hand side is equal to zero. This zero equality follows from the fact that the curvature is constant and hence can be taken outside the integration, by employing (A 7) of the Appendix.

The reason that the integral (2.13) cannot be applied straightforwardly is due to the fact that the outer normal of the boundary is an eigenfunction of the *adjoint* of the double-layer potential integral (see also the Appendix). As was stated in Pozrikidis (1992, p. 110), the double-layer potential is capable of representing a flow that contains sinks/sources, but sometimes the adjoint double-layer potential's outer normal eigenvalue has to be removed. The method of deflating the boundary normal as described by both Kim & Karrila (1991) and Pozrikidis (1992) cannot be applied straightforwardly here, since they consider resistance and movement problems of solid and liquid particles in the fluid only. Therefore, we will briefly outline the further deflation of (2.13) that is used in this paper for the case of vanishing holes.

In a similar way as the integral formulation (2.7) is obtained from the fundamental solution which represents a point force in an infinite two-dimensional fluid, cf. van de Vorst *et al.* (1992), an integral equation can be obtained that represents a sink at a particular place. Consider this equation for an *arbitrary* point, say $x^m$, inside the area surrounded by the hole $\Gamma_m$ ($m = 1,\ldots,M$). Hence we obtain $M$ equations which after summation reduce to the following integral formulation that models all those sink contributions, i.e.

$$\sum_{m=0}^{M} \int_{\Gamma_m} \hat{q}_j v_j \,\mathrm{d}\Gamma_y = \sum_{m=0}^{M} \int_{\Gamma_m} \kappa \hat{u}_j n_j \,\mathrm{d}\Gamma_y, \tag{2.14}$$

where

$$\hat{q}_j(y) = \frac{1}{\pi} \sum_{m=1}^{M} \left( \frac{2r_j^m}{(R^m)^4} r_i^m n_i - \frac{\delta_{ji} n_i}{(R^m)^2} \right), \qquad \hat{u}_j(y) = -\frac{1}{2\pi} \sum_{m=1}^{M} \frac{r_j^m}{(R^m)^2}, \tag{2.15}$$

and $r_i^m = x_i^m - y_i$ and $R^m = |x^m - y|$. Note that the same integral equation will be

obtained when there are sources modelled inside the hole areas. Hence (2.14) is suited to model both the shrinking and expansion of inner holes. The above integral is applied as a constraint on the solution of (2.13), i.e. we seek a velocity field $\boldsymbol{v}$ that satisfies both the integrals (2.13) and (2.14).

The integral (2.14) can be applied in order to deflate (2.13) with respect to the outer normal in the following way,

$$c_{ij}v_j(\boldsymbol{x}) + \sum_{m=0}^{M}\Big(\int_{\Gamma_m} q_{ij}(\boldsymbol{x},\boldsymbol{y})v_j\,\mathrm{d}\Gamma_y + n_i(\boldsymbol{x})\int_{\Gamma_m}\hat{q}_j v_j\,\mathrm{d}\Gamma\Big) + \varphi_i^{pk}(\boldsymbol{x})\int_{\Gamma_p}\varphi_j^{pk}v_j\,\mathrm{d}\Gamma$$
$$= \sum_{m=0}^{M}\Big(\int_{\Gamma_m}\kappa u_{ij}(\boldsymbol{x},\boldsymbol{y})n_j\,\mathrm{d}\Gamma + n_i(\boldsymbol{x})\int_{\Gamma_m}\kappa\hat{u}_j n_j\,\mathrm{d}\Gamma\Big), \quad (\boldsymbol{x}\in\Gamma_p). \tag{2.16}$$

In the Appendix, it is shown that the solution of the above equation satisfies both the requirements (2.13) and (2.14). Hence this formulation provides the correct solution in order to simulate the sintering of multiply connected domains.

### 2.3. *Numerical solution*

As mentioned before, a boundary element method (BEM) is employed to solve (2.16). Details of this implementation for the case of a simply connected domain can be found in Van de Vorst *et al.* (1992) and van de Vorst & Mattheij (1992*a*,*b*). For multiply connected domains the discretization of the governing integral equations is straightforward too.

Let the total boundary be discretized in say $N$ nodal points. After applying the BEM to (2.16) we obtain a square full rank system of $2N \times 2N$ algebraic equations that is denoted by

$$\boldsymbol{H}\vec{v} = \boldsymbol{G}\vec{b}. \tag{2.17}$$

Here $\vec{v}$ and $\vec{b}$ are the velocity and surface tension ($=\kappa\boldsymbol{n}$) respectively of all successive nodal points. Since the vector $\vec{b}$ is known, this system can be solved by simple Gaussian elimination with partial pivoting.

After solving the above system of equations we have to perform a time step. More precisely, we actually have to solve a system of $2N$ nonlinear Ordinary Differential Equations (ODEs). Using (2.6), which describes the movement of the material boundary points, this system can be described by

$$\dot{\vec{x}} = \boldsymbol{H}^{-1}(\vec{x})\,\boldsymbol{G}(\vec{x})\,\vec{b}(\vec{x}), \tag{2.18}$$

where $\vec{x}$ is the vector of all successive nodes and the dot denotes the derivative with respect to the time.

In the available literature about free creeping Stokes flows this system of ODEs is discretized by a simple forward Euler scheme or other explicit schemes. However, it appears that the above system of ODEs can be *stiff* for certain type of shapes (e.g. shapes which have cusps); in such a case the time step in the forward Euler scheme has to be taken very small to obtain a stable method. Therefore, we have implemented a variable-step, variable-order Backward Differences Formulae (BDF) method to solve those ODEs. More details can be found in van de Vorst & Mattheij (1992*a*).

The collocation points of the boundary are (re)distributed after a certain number of time steps. In van de Vorst & Mattheij (1992*b*), we proposed an algorithm for a fairly optimal node redistribution based on equidistributing the curvature of the boundary. The aim of that algorithm is twofold. Firstly, the number and position of the discretization points are optimized, which is important because the computational

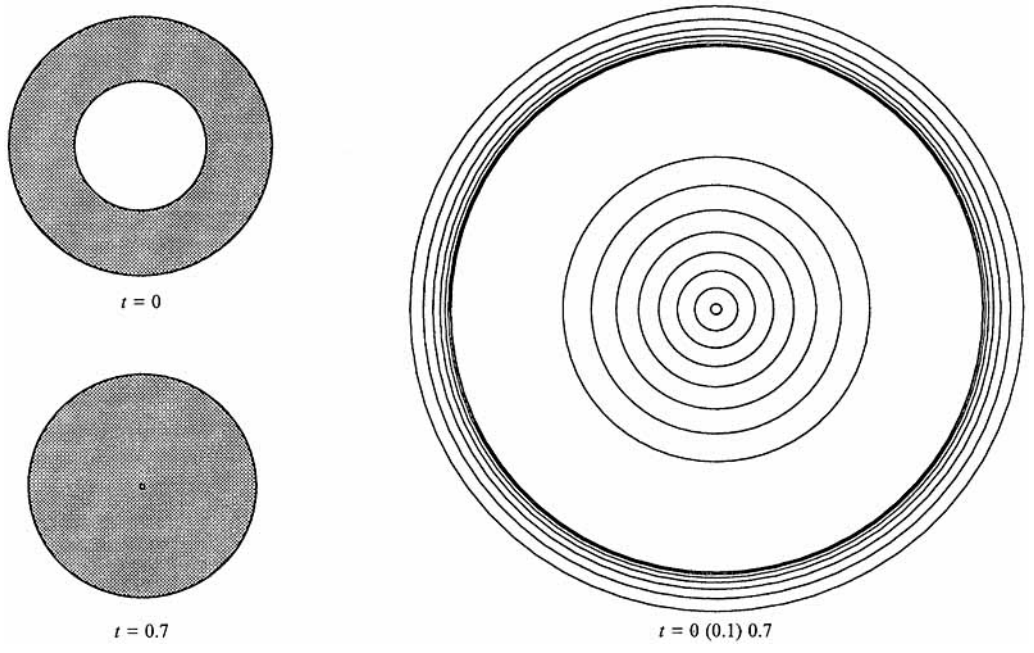


FIGURE 1. The shrinkage of a circular disk with a circular hole centred at the origin.

costs per time step are proportional to $(2N)^3$. Secondly, the algorithm treats regions with a large curvature 'cusp' so that the curvature of this particular region is preserved after the redistribution to avoid (numerical) oscillations in the computed velocity field.

## 3. Results and discussion

In this section we show the numerical results obtained by simulating a number of sintering geometries using the integral formulation described in the previous section. Since the driving force for sintering arises from the excess free surface energy, a particular shape will minimize its boundary during the deformation. Because of this, a two-dimensional fluid region transforms itself into a circle when time is increasing. From the incompressibility of the fluid it follows that during this deformation the total area of the domain has to remain constant.

Firstly, we will compare the solution method to the analytical solution for the possibly most simple geometry: a circular disk with circular hole centred at the origin. Afterwards, we demonstrate the method for several other multiply connected domains. In particular, we will consider the sintering of particle packings that consist of a number of equal cylinders. It will be shown that those simulations provide a justification for the use of unit problems in the theory of sintering. All simulations have *linear* boundary elements applied and are carried out on a SUN Sparc+1 workstation; the error in the total area of the domains was always less than 1% (which should be a conserved quantity).

### 3.1. *The sintering of a circular disk with a circular hole*

The first example that we consider is the evolution of a circular fluid disk with a circular hole centred at the origin. We denote by $r_o$ the radius of the outer circle and

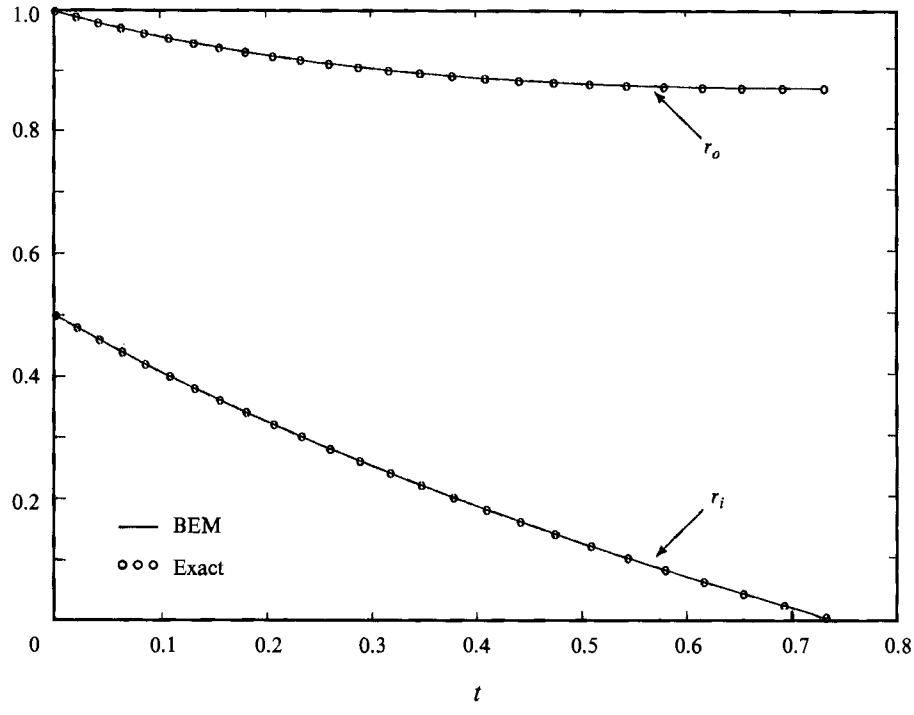


FIGURE 2. The numerically found behaviour of the inner and outer radius of the circular disk, which matches very well with the exact analytical solution.

by $r_i$ the inner radius. For this fluid domain, the solution of the Stokes equations can be found after transformation to cylindrical coordinates ($r\cos\theta, r\sin\theta$). One obtains for the radial velocity

$$v_r(r) = \frac{r_o r_i}{2(r_i - r_o)r}, \qquad r_i \leqslant r \leqslant r_o. \tag{3.1}$$

From this solution and the condition $r_o > r_i$, it follows that the interior circular region vanishes when time is increasing.

From this analytical solution for the radial fluid velocity, we can deduce the exact solution for the inner and outer radius as functions of time also. Using both that the fluid surface remains constant and the Lagrangian representation (2.6) for the velocity, we obtain the following ordinary differential equations for the inner and outer radius respectively:

$$\left.\begin{aligned} \dot{r}_i &= \frac{(3+4r_i^2)^{\frac{1}{2}}}{2\left(2r_i - (3+4r_i^2)^{\frac{1}{2}}\right)}, \qquad r_i(0) = R_i, \\ \dot{r}_o &= \frac{(4r_o^2-3)^{\frac{1}{2}}}{2\left((4r_o^2-3)^{\frac{1}{2}} - 2r_o\right)}, \qquad r_o(0) = R_o. \end{aligned}\right\} \tag{3.2}$$

We obtain for the solution of those equations

$$t = 2(R_i - r_i) + (3+4r_i^2)^{\frac{1}{2}} - (3+4R_i^2)^{\frac{1}{2}}, \tag{3.3}$$

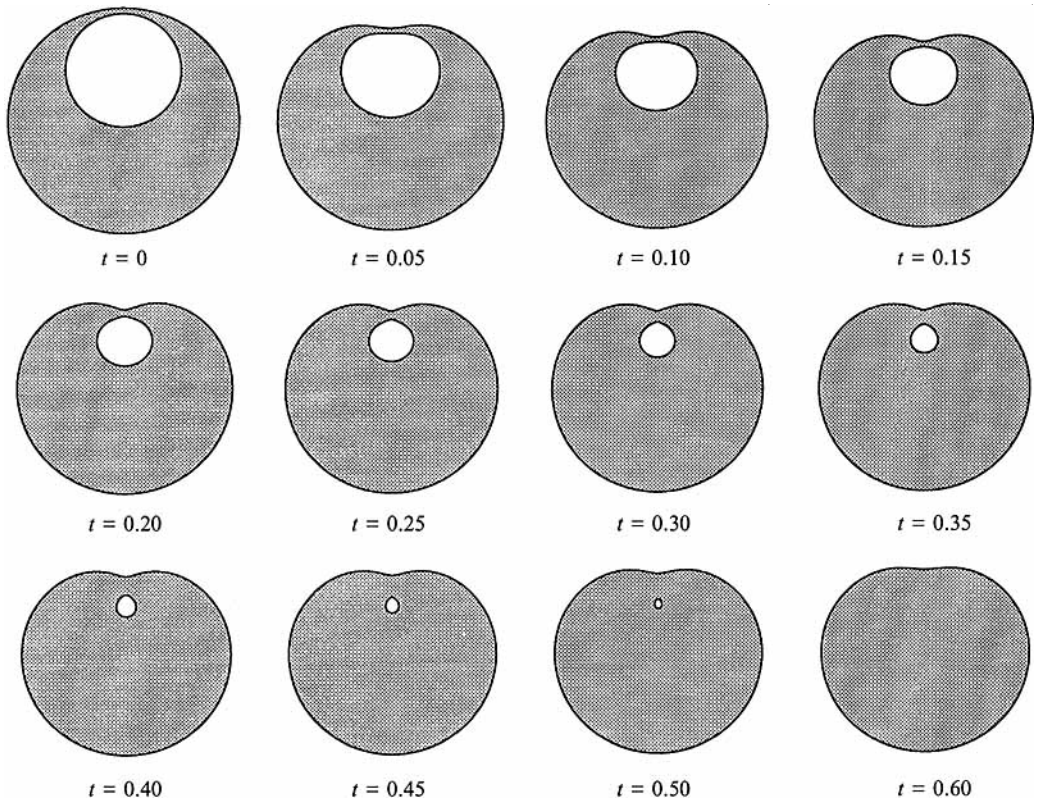


FIGURE 3. The shrinkage of a circular hole which is located close to the outer boundary of a circular disk. The hole remains in the fluid region and will disappear after a period of time.

and

$$t = 2(r_o - R_o) - (4r_o^2 - 3)^{\frac{1}{2}} + (4R_o^2 - 3)^{\frac{1}{2}}. \tag{3.4}$$

The initial outer radius ($R_o$) of the disk is taken equal to 1 and the inner radius ($R_i$) is set to 0.5. In figure 1 we have plotted the shrinkage of the circular hole as time increases. Both the initial geometry and the shape at time $t = 0.7$ are plotted. The evolution of the hole is also plotted after successive periods of 0.1. As can be observed, the internal hole shrinks and disappears after a certain period of time: the domain is becoming simply connected.

In figure 2 are shown the exact solutions (3.3) and (3.4) compared with the numerically found shrinkage of the hole. As can be observed, the numerical and analytical solutions match very well. The moment that the hole disappears is also obtained by the simulation reasonably well: from (3.3) and using $r_i = 0$, we derive that the hole is filled up exactly at $t = \sqrt{3} - 1 \approx 0.73$; the latter approximation was found by the numerical code.

Next, we consider the evolution of a similar circular hole that is situated close to the outer boundary of the fluid domain. The interesting question in this particular geometry is whether the hole is going outside the fluid, i.e. whether the domain will become simply connected. In order to simulate this problem, we have taken the initial geometry plotted in figure 3. The circular fluid disk has radius 1 and is centred at the

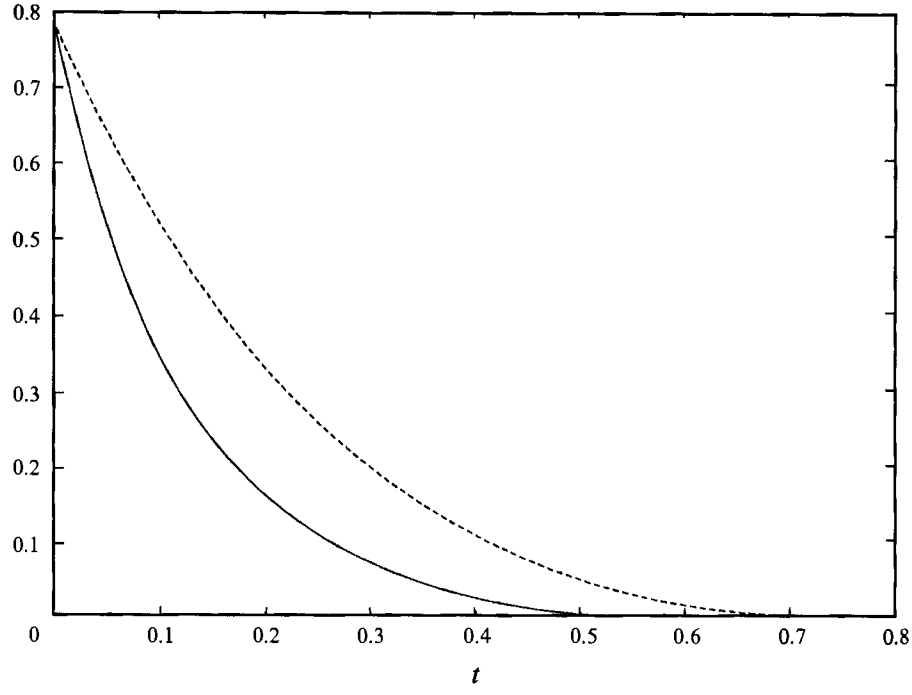


FIGURE 4. The shrinking of the hole surface from a circular disk that is centred at the origin (dashed line) compared to the hole area shrinkage of a similar sized hole that is situated close to the outer boundary (solid line).

origin. For the circular hole we have taken an initial radius of 0.5 and the midpoint of the hole is situated at $x_2 = 0.45$ on the vertical axis. Thus, the closest distance of the hole to the outer boundary is 0.05.

In figure 3 the fluid domain at times $t = 0(0.05)0.50$ is shown. As can be seen, the hole *remains* in the fluid domain. A small disturbance in the neighbourhood of the closest part to the hole is the only effect on to the outer boundary. The hole remains in the fluid domain and is completely filled up by fluid at time $t = 0.6$.

Another interesting phenomenon demonstrated by this geometry is that the shrinkage rate of this particular hole is faster than a similar hole that is centred at the origin. Note that those geometries contain both the same amount of fluid and an equally sized interior hole. Only the position of the centre of these holes differs. In figure 4 the interior area shrinkage of both holes is plotted. As can be seen, the shrinking rate of the hole that is positioned closest to the outer boundary proceeds faster than the hole of the other fluid domain. An explanation for this difference is that for a centred hole all the fluid has to be moved in the direction of the origin. In the other case, there is not much flow occurring in the bottom part of the shape; the hole is mainly filled up by fluid flow that appears in the upper part of the domain.

### 3.2. *The sintering of an elliptic hole*

The second example is the deformation of a circular disk with an elliptic hole centred at the origin. This particular example is chosen since Hopper (1991) analytically solved the shrinkage of an elliptic hole in an infinite region of fluid. From that

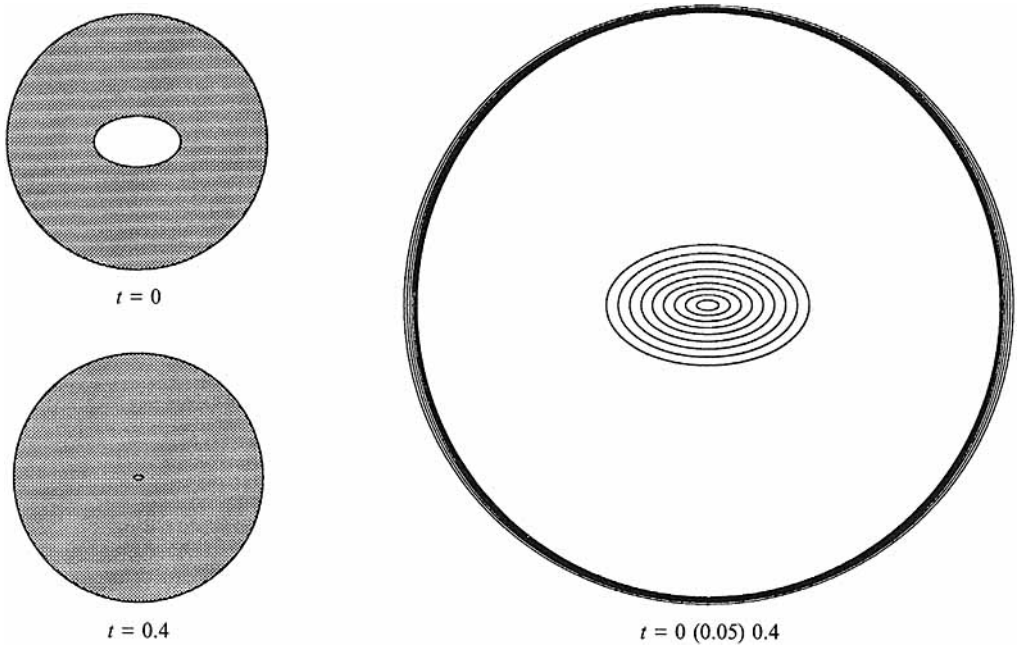


FIGURE 5. The shrinkage of a circular disk with an elliptic hole centred at the origin.

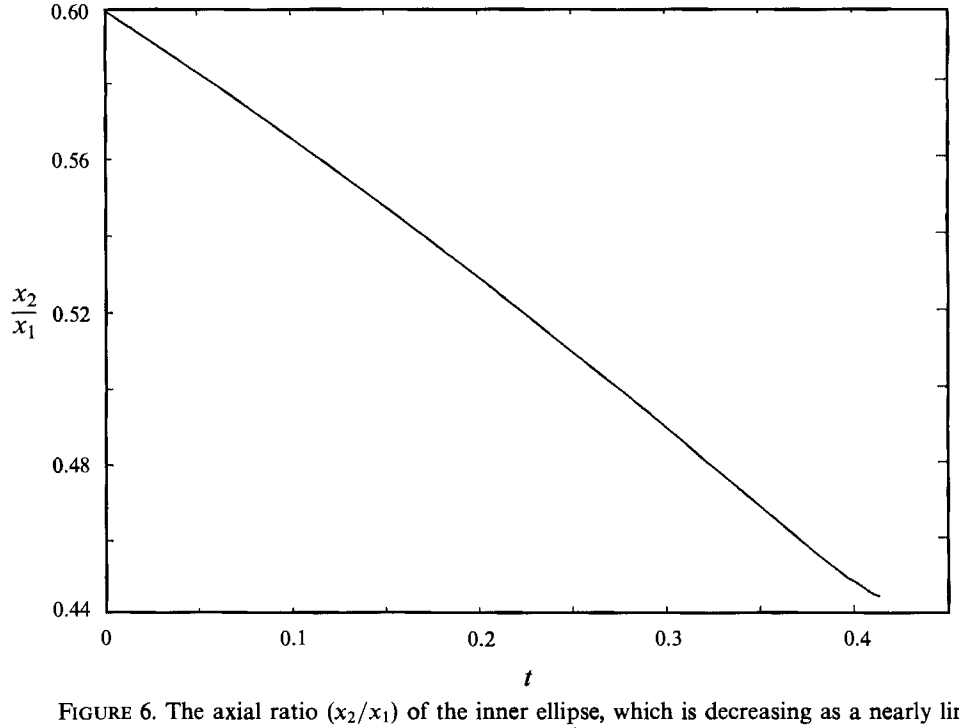


FIGURE 6. The axial ratio $(x_2/x_1)$ of the inner ellipse, which is decreasing as a nearly linear function of time.

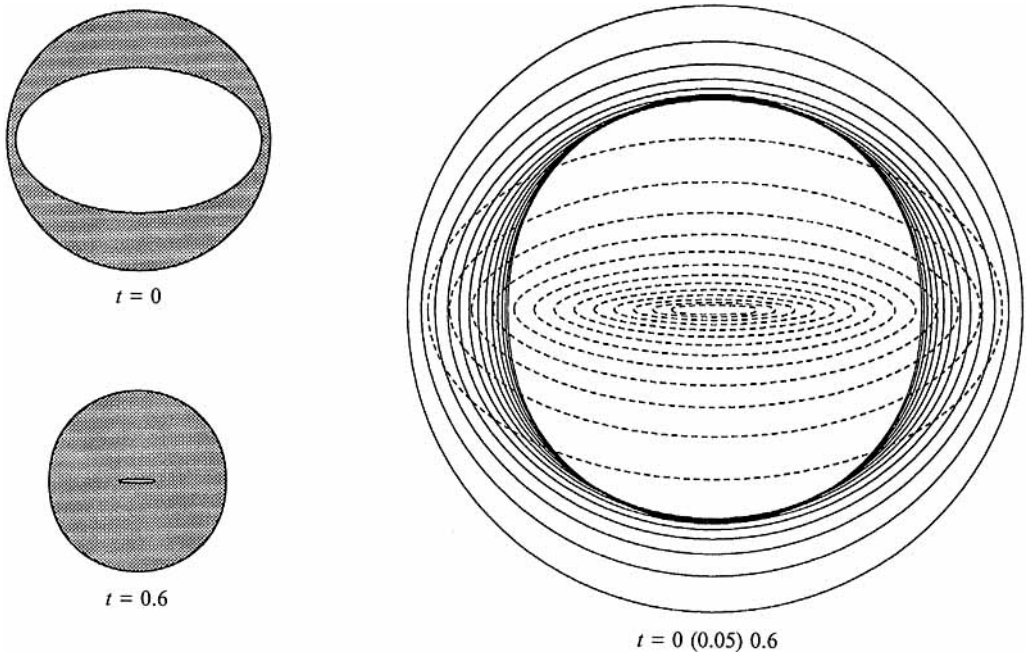


FIGURE 7. The shrinkage of a circular disk with an elliptic hole centred at the origin when the ends of the initial ellipse are close to the outer boundary.

solution, he found that an elliptic hole shrinks at a constant rate with a constant aspect ratio. Here, we approximate the infinite region by a circular disk. The radius of the disk is set equal to 1 and the ellipse is described by $9x_1^2 + 25x_2^2 = 1$.

In figure 5 we have plotted this particular initial shape and also the shape at time $t = 0.4$. Furthermore, the deformation is shown at times $t = 0(0.05)0.4$. The latter plot shows that the shrinkage of the inner boundary proceeds as an elliptic hole, which is similar to what was obtained by Hopper (1991) for the infinite fluid region case. In figure 6 we show the development of the axial ratio $(x_2/x_1)$ of this inner ellipse as a function of time. As can be seen in the figure, this is an almost *linear* decreasing function of time, even when the hole has reached the moment of vanishing. This result differs from the behaviour that Hopper (1991) derived for the elliptic hole in an infinite region, i.e. he found a *constant* aspect ratio during the evolution.

This linear decreasing of the axial ratio is valid only when the ends of the ellipse are not to close to the outer boundary. This is illustrated in figure 7. Here, we have plotted the evolution of an enlarged elliptic hole in a similar sized circular disk at times $t = 0(0.05)0.6$. The elliptic hole is described by the equation $(\frac{3}{2.8})^2x_1^2+(\frac{5}{2.8})^2x_2^2 = 1$, thus the starting axial ratio is equal to that of the elliptic hole of figure 5. The figure shows that the shrinkage of the interior hole proceeds as ellipse-like shapes too. This plot illustrates also that an elliptic hole, if large enough, will shrink to a line contact at later times.

The axial ratio of this elliptic hole does not decrease at a linear rate as can be observed from figure 8. This different behaviour can be attributed to the influence of the outer boundary at the ends of the ellipse. We already observed such an effect of the outer boundary on the hole deformation in the previous subsection for the

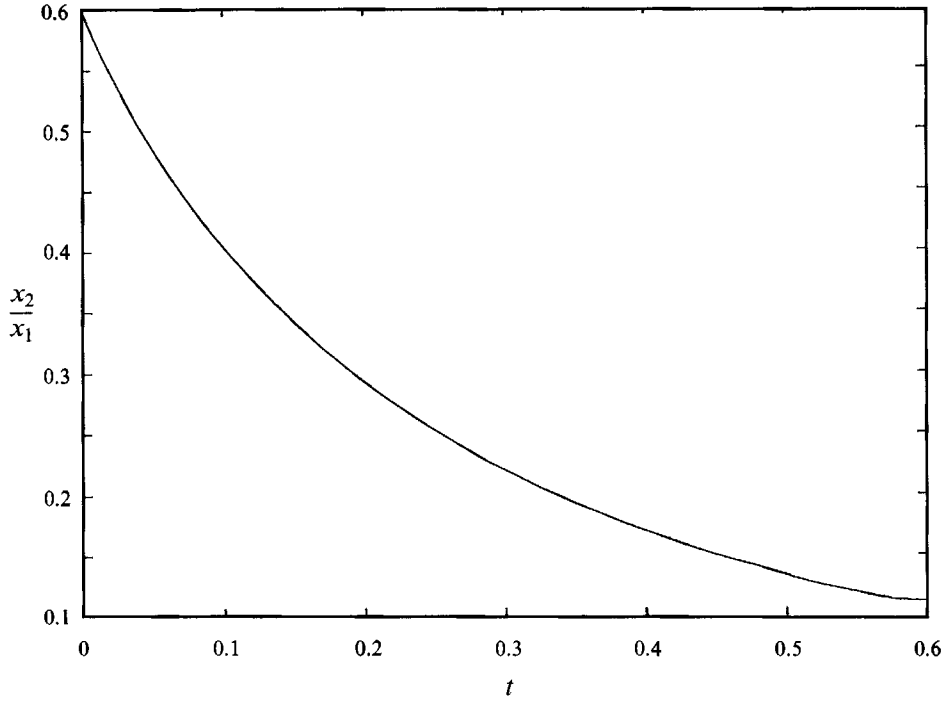


FIGURE 8. The axial ratio $(x_2/x_1)$ of the inner ellipse of figure 7 as a function of time. This ratio does not decrease at a linear rate since the outer boundary influences the shrinking of the hole.

shrinkage rate of an eccentric-circular annulus. Therefore, an explanation of this effect can be obtained by using similar arguments as mentioned in that subsection.

### 3.3. *The sintering of cylindrical packings*

Thus far, the fluid domains that we have considered are shapes with a moderately well-behaved boundary curvature. It is also possible to simulate the evolution of geometries with a more extreme boundary curvature. In order to demonstrate this, we consider some cylindrical packings. In those packings, the cylinders already make contact with each other.

In sintering literature, the rate of contact between two coalescing cylinders may be quantified by the contact radius and the touching region near the neck. This contact radius, say $\rho$, is a measure of how strong a sintering compact already is. When the contact radius is small, a smaller force will be necessary to break the contact between both cylinders than at later stages of the sintering process. When a cell structure is determined that may be considered as a representation of a sintering compact, the coalescing rate can also be used to obtain a better phenomenological insight into the shrinkage of such a macroscopic system. As we mentioned in the introduction, the contact radius development can be theoretically studied by unit problems. Here, in particular, we consider the unit problem of the coalescence of two equal cylinders. The simulations below will show that such a theoretical simplification is justified in order to describe the development of a more complex sintering compact.

In the following examples we have set the initial radii of all cylinders equal to 0.5. The contact radius between two touching cylinders was initially taken equal to 0.095 for all neck regions. Furthermore, we used the analytical solution for the

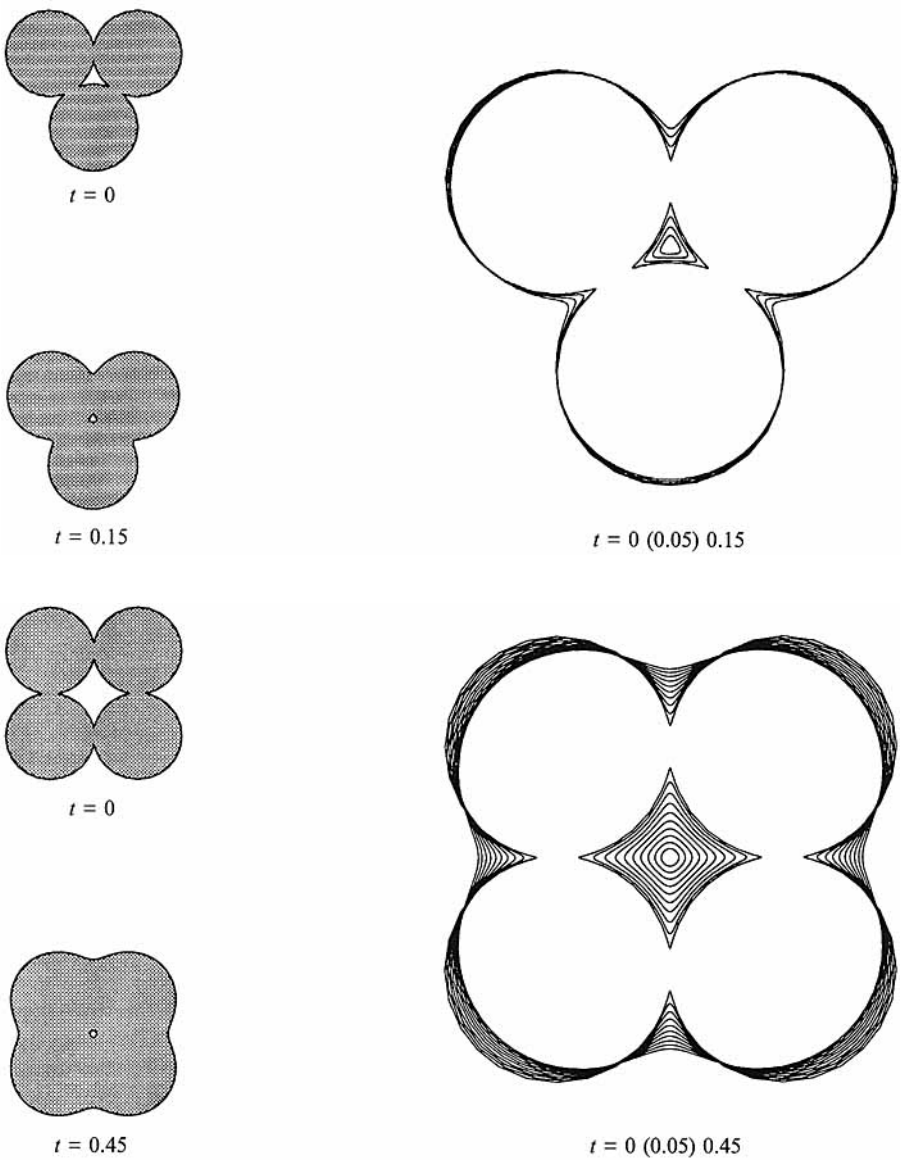


FIGURE 10. The deformation of four regular packed cylinders.

coalescence of two equal cylinders to approximate the neck regions of the initial shape. This analytical solution is derived by Hopper (1990, §4.4). However, this particular solution is valid for the coalescence of two equal cylinders with both initial radii $\frac{1}{2}\sqrt{2}$. It is straightforward to obtain the solution for the coalescence of two equal cylinders with an arbitrary initial radius, cf. van de Vorst & Mattheij (1992*b*).

In figures 9–12 we plot the deformation of three to six symmetrically placed equal sized cylinders with a hole in the interior of the domain. All initial shapes are constructed so that the mid-points of the cylinders are equally distributed on a circle centred in the origin. The radius of this circle is chosen so that the distance between

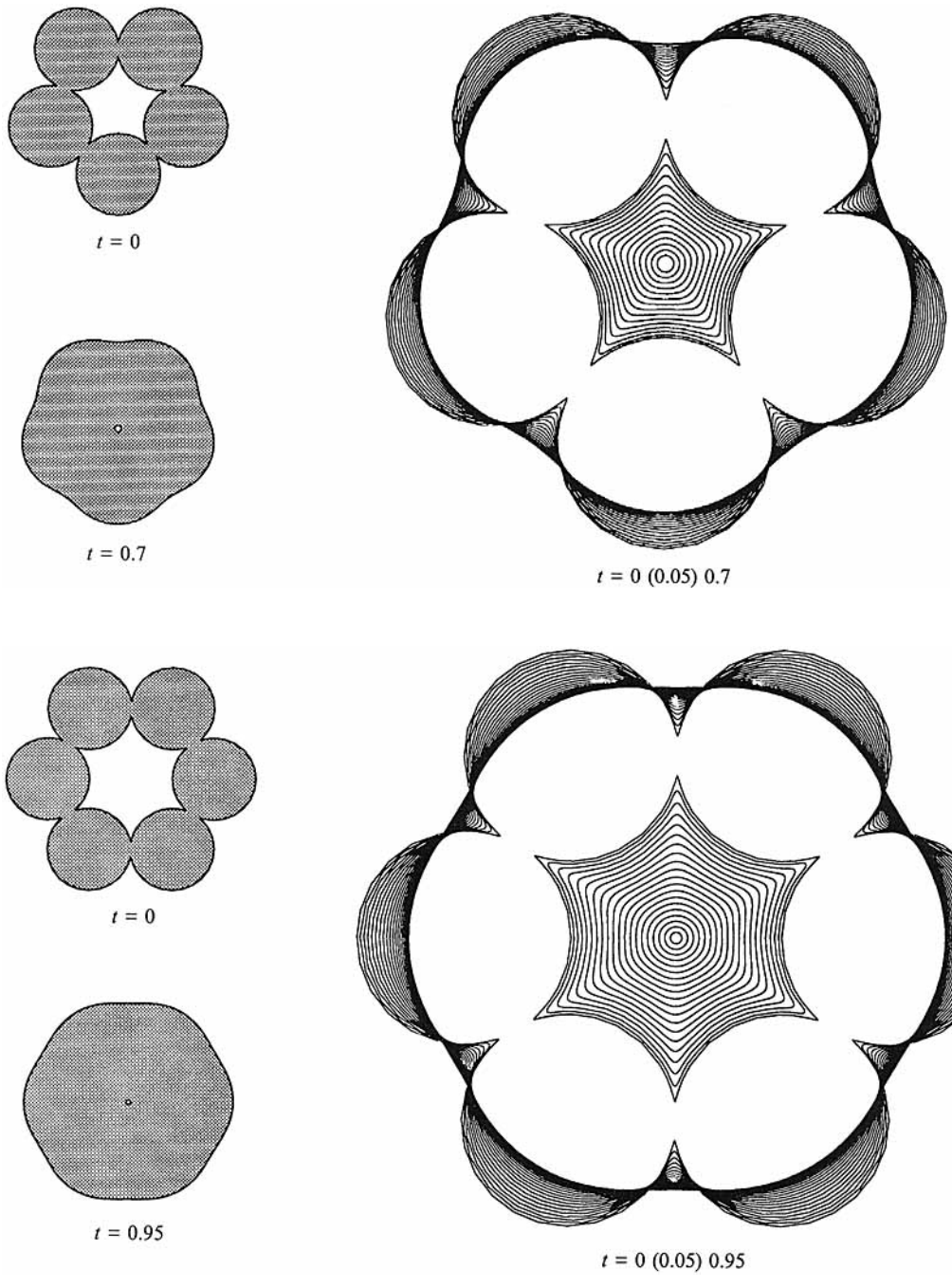


FIGURE 12. The deformation of six regular packed cylinders.

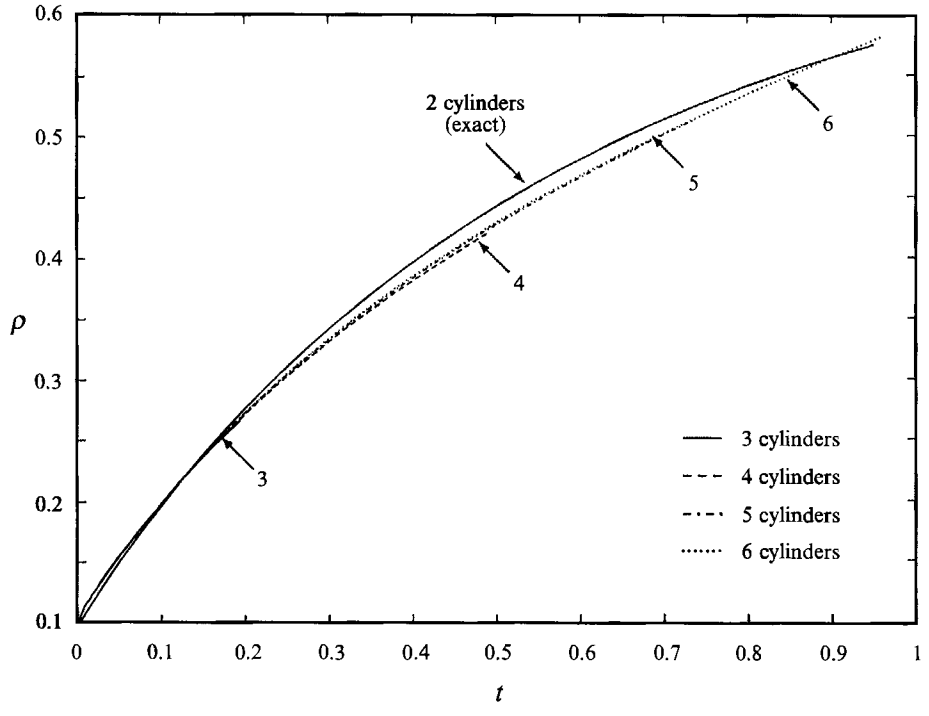


FIGURE 13. The development of the contact radius ($\rho$) between two cylinders of the packings of the figures 9-12 compared with the exact neck growth of two coalescing cylinders.

two successive cylindrical mid-points is equal to the exact shrinkage of two coalescing cylinders.

An interesting question is the behaviour of the neck growth between two touching cylinders of these packings compared with the exact contact radius of two coalescing cylinders. In figure 13 is shown the development in time of the contact radius for all the four packings. In this figure, the contact radius is plotted from the neck regions that are situated along the positive vertical axis. The exact neck radius for the coalescence of two cylinders with initial radii equal to 0.5 is also plotted.

From this picture we see that the neck growth for all the four cases is of the same rate and almost equal to the contact radius development of two coalescing cylinders. From this observation we conclude that the sintering of the above packings, in fact, can reasonably be described by considering the model of the coalescence of two equal cylinders. This illustrates the importance of the exact analytical solution for this particular coalescence as has been obtained by Hopper. Furthermore, we observe that there is even no change in the coalescing rate at times when the internal holes have almost vanished.

These numerical experiments may also give some justification of the modelling of the densification of powder compacts based on such unit problems. An example of such a model based on unit problems that describes the deformation of a sintering compact was recently presented by Jagota & Dawson (1988*b*). In that model, the particle packing is modelled as a framework of links between touching spheres, and the development of those links are described by using the behaviour of the unit problem of two coalescing spheres separately.

The shrinking of the interior holes from the packings of figures 9–12 shown in

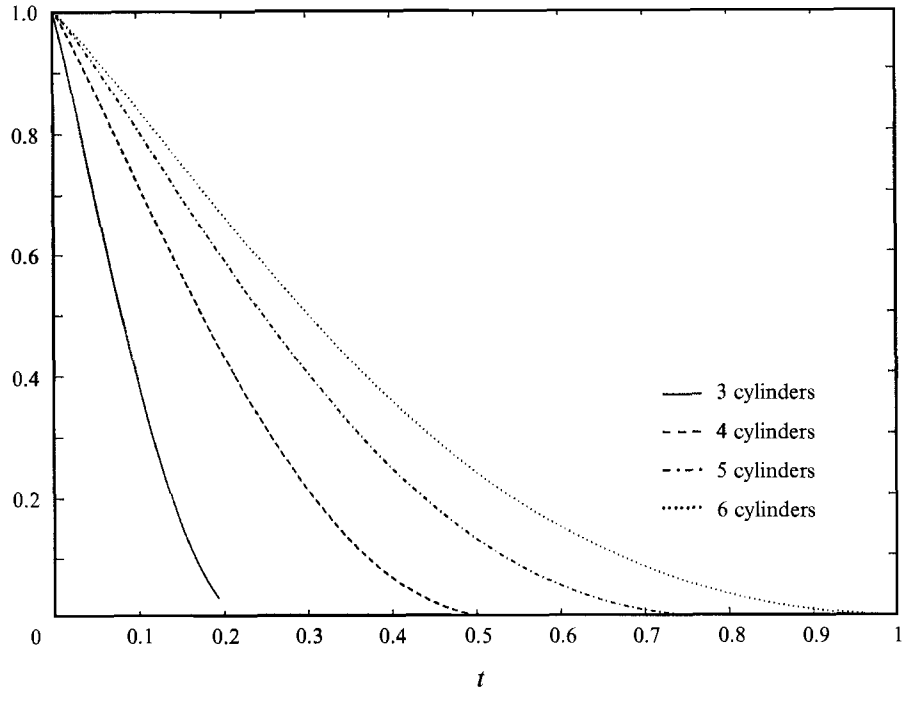


FIGURE 14. The shrinking of the interior hole area from the packings of the figures 9-12. The hole area is normalized by the initial hole surface.

figure 14. In this graph, the interior hole area is normalized by the initial hole surface. From this figure we observe that all the holes are monotonically decreasing in time. They even initially decrease at a *same rate*. This latter observation can be clarified by noting that in the initial stage there is only large flow activity in the neighbourhood of the touching area between two successive cylinders which will not influence the hole surface much.

Up to now, the shapes considered were all doubly connected domains. In order to demonstrate the method for a really multiply connected region, we consider the packing of a $4 \times 4$ array of cylinders. Again all the contact radii are set equal to 0.095. In figure 15 we show the sintering of this particular compact. In the picture on the right of this figure is shown the deformation at equal periods of 0.05. It can be seen that the holes are moving further into the interior of the fluid.

In figure 16 we have set the initial neck radii in the vertical direction equal to 0.3. Because of this, the sintering is faster. As can be observed in the right plot of this figure, the holes deform into an ellipse-like shape. When we compare the movement of these holes with the movement in figure 15, it can be seen that they are situated almost at the same place at the final time. This implies that the movement is faster.

## 4. Conclusion

The examples shown in the previous subsections illustrate that with the method presented we are able to simulate all kinds of two-dimensional multiply connected domains. The main limitation in these simulations is the computer resources; also we cannot yet deal with cases where boundaries touch during a simulation.

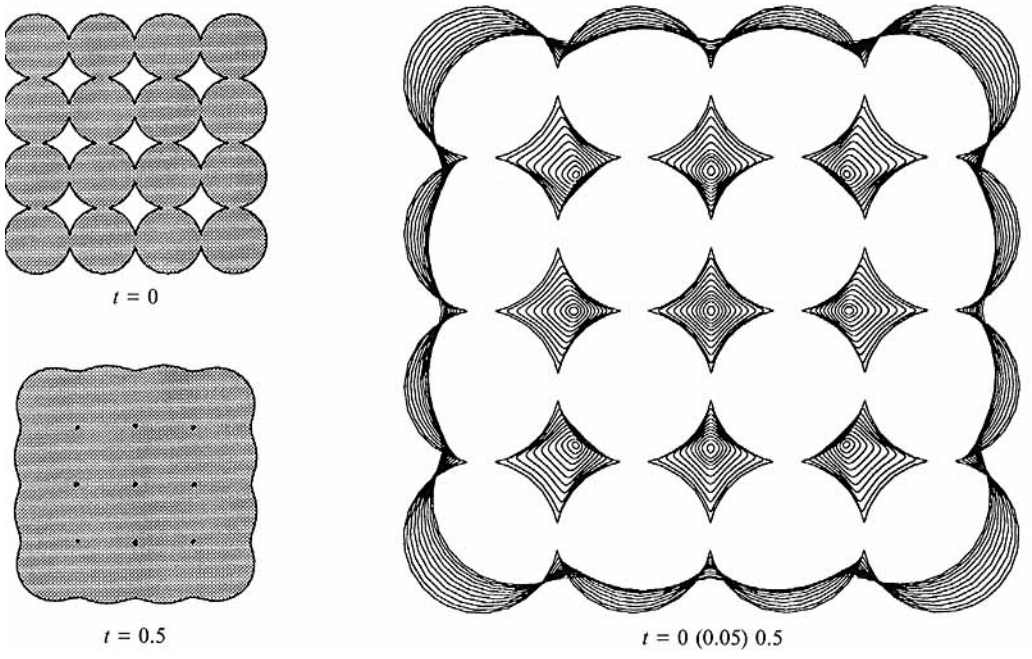


FIGURE 15. The sintering of a regular 4 × 4 array of cylinders with initially equal contact radii between all cylinders.

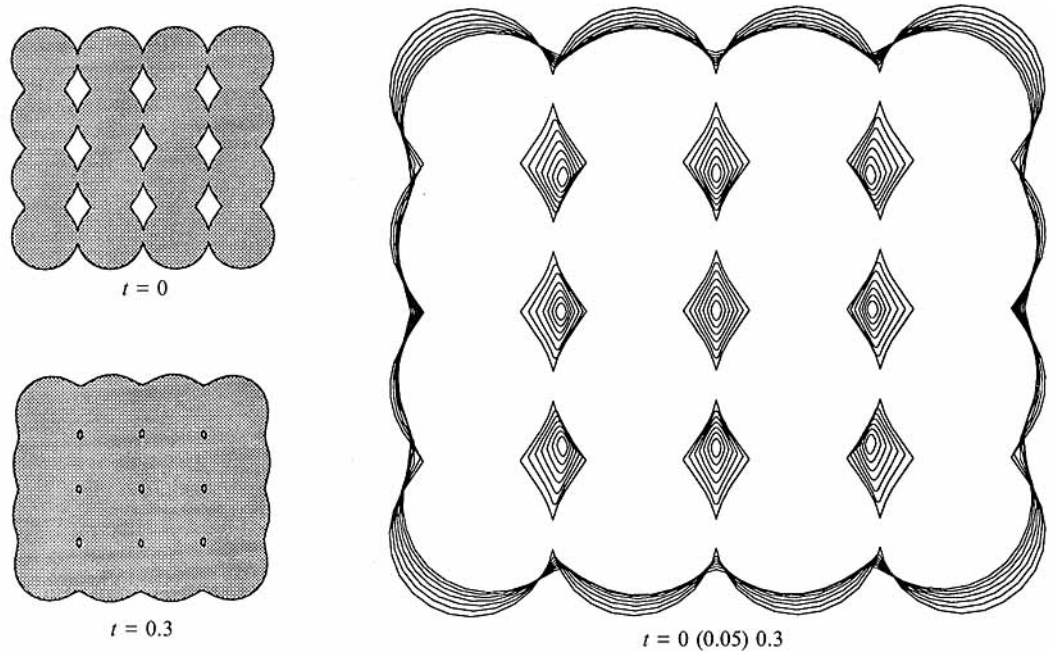


FIGURE 16. The sintering of a 4 × 4 array of cylinders. The initial contact radius between the cylinders in the vertical direction is set more than three times larger than in the horizontal direction.

It is obvious that some experimental verification has to be performed to justify this model. Starting in two dimensions, such experiments should consider the sintering of a packing of well-controlled glass fibres that can be compared with the numerical simulation of that particular packing.

Recently, Korwin *et al.* (1992) performed experments in which they considered the sintering of two equal sized glass fibres. The results obtained were compared with Hopper's analytical solution and look very promising. Because of this, these experiments also provide a (little) justification of our numerical approach.

The author thanks Dr C. Pozrikidis of the University of California at San Diego for some valuable comments concerning this paper. Professor R.M.M. Mattheij is also thanked for critically reading the manuscript. This research was supported by the Technology Foundation (STW).

## Appendix A. Justification of the integral formulation employed

In this appendix we show that the solution $\boldsymbol{v}$ of the deflated integral formulation (2.16) satisfies both the requirements (2.13) and (2.14). We will achieve this result by describing the single- and double-layer potentials involved in terms of functional operators. The precise mathematical justification of what follows will be omitted. The reader may ignore the functional operators too and consider those as matrix operations.

Let $\mathbf{G}_m$ be the single-layer potential operator with a continuously varying density $\boldsymbol{\phi}(\boldsymbol{y})$ subjected to the boundary $\Gamma_m$, i.e.

$$(\mathbf{G}_m\boldsymbol{\phi})_i = \int_{\Gamma_m} \frac{1}{4\pi}\left[-\delta_{ij}\log R + \frac{r_i r_j}{R^2}\right]\phi_j \,\mathrm{d}\Gamma_y. \tag{A 1}$$

The double-layer potential $\mathbf{H}_m$ with density $\boldsymbol{\psi}(\boldsymbol{y})$ is defined analogously,

$$(\mathbf{H}_m\boldsymbol{\psi})_i = \int_{\Gamma_m} \frac{r_i r_j r_k}{\pi R^4}\psi_k n_j^m \,\mathrm{d}\Gamma_y, \tag{A 2}$$

where $\boldsymbol{n}^m$ denotes the normal to $\Gamma_m$ pointing out of the fluid. Moreover, the boundary $\Gamma_m$ is followed in a counter-clockwise direction. The functional inner product is defined in the usual way,

$$\langle\boldsymbol{\phi},\boldsymbol{\psi}\rangle_m = \int_{\Gamma_m} \phi_i\psi_i \,\mathrm{d}\Gamma, \tag{A 3}$$

and the adjoint of an operator $\mathbf{A}$ is defined as, cf. Kreyszig (1978),

$$\langle\boldsymbol{\phi},\mathbf{A}\boldsymbol{\psi}\rangle = \langle\mathbf{A}^*\boldsymbol{\phi},\boldsymbol{\psi}\rangle, \tag{A 4}$$

where the asterisk denotes the adjoint. Here the adjoint of the operators (A 1) and (A 2) can be found by transposing the indices $j$ and $k$ and swapping the arguments $\boldsymbol{x}$ and $\boldsymbol{y}$, i.e.

$$(\mathbf{G}_m^*\boldsymbol{\phi})_i = (\mathbf{G}_m\boldsymbol{\phi})_i, \qquad \text{and} \qquad (\mathbf{H}_m^*\boldsymbol{\psi})_i = -n_k^m(\boldsymbol{x})\int_{\Gamma_m} \frac{r_i r_j r_k}{\pi R^4}\psi_j \,\mathrm{d}\Gamma_y. \tag{A 5}$$

Hence $\mathbf{G}$ is a *self-adjoint* linear operator. Furthermore, we require the following identities that apply on the potentials in relation to the outer normal:

$$\left(\mathbf{H}^*\boldsymbol{n}\right)_i = \left(-n_j(\boldsymbol{x})\mathbf{H}\boldsymbol{e}^j\right)_i = \begin{cases} n_i, & \boldsymbol{x} \text{ inside } \Gamma \\ \frac{1}{2}n_i, & \boldsymbol{x} \text{ on } \Gamma \\ 0, & \boldsymbol{x} \text{ outside } \Gamma, \end{cases} \tag{A 6}$$

where $e^j = (\delta_{1j}, \delta_{2j})^T$. Hence the outer normal $\boldsymbol{n}$ is an eigenfunction of the adjoint operator $\mathbf{H}^*$. For the single-layer potential it can be found that

$$\left(\mathbf{G}\boldsymbol{n}\right)_i = \int_\Gamma u_{ij} n_j \, d\Gamma = \int_\Omega \nabla \cdot \boldsymbol{u}^i \, d\Omega = 0, \tag{A 7}$$

which is derived by applying both the divergence theorem of Gauss and that $\boldsymbol{u}^i = (u_{i1}, u_{i2})^T$ is the fundamental solution of the Stokes problem due a point force in the $e^i$-direction. Hence the incompressibility condition is fulfilled. The projection operator $\mathbf{P}_m$ is defined by

$$\mathbf{P}_m = \sum_{k=1}^{3} \boldsymbol{\varphi}^{mk}(\boldsymbol{x}) \langle \cdot, \boldsymbol{\varphi}^{mk} \rangle_m,$$

which is a self-adjoint operator. The integral formulation (2.13) can now be written in the above operator notation as

$$\left.\begin{aligned} \left(\tfrac{1}{2}\mathbf{I} + \mathbf{H}_0 + \mathbf{P}_0\right)\boldsymbol{v}^0 - \sum_{j=1}^{M} \mathbf{H}_j \boldsymbol{v}^j &= \sum_{j=0}^{M} \mathbf{G}_j \boldsymbol{b}^j \quad (\boldsymbol{x} \in \Gamma_0), \\ \mathbf{H}_0 \boldsymbol{v}^0 - \sum_{j=1}^{M} \mathbf{H}_j \boldsymbol{v}^j + \left(\tfrac{1}{2}\mathbf{I} + \mathbf{P}_m\right)\boldsymbol{v}^m &= \sum_{j=0}^{M} \mathbf{G}_j \boldsymbol{b}^j \quad (\boldsymbol{x} \in \Gamma_m), \end{aligned}\right\} \tag{A 8}$$

where $\boldsymbol{v}^m$, $\boldsymbol{b}^m = \kappa \boldsymbol{n}^m$ are the velocity and tension function respectively of the boundary $\Gamma_m$ and $\mathbf{I}$ is the indentity operator. At a similar way, we denote (2.14) by

$$\mathbf{h}_0 \boldsymbol{v}^0 - \sum_{j=1}^{M} \mathbf{h}_j \boldsymbol{v}^j = \sum_{j=0}^{M} \mathbf{g}_j \boldsymbol{b}^j, \tag{A 9}$$

where

$$\mathbf{g}_m \boldsymbol{\phi} = \int_{\Gamma_m} \hat{u}_j \phi_j \, d\Gamma_y, \qquad \mathbf{h}_m \boldsymbol{\psi} = \int_{\Gamma_m} \hat{q}_j \psi_j \, d\Gamma_y,$$

and $\Gamma_m$ is considered in a counter-clockwise direction. From (A 8) and (A 9), we obtain for the deflated formulation (2.16)

$$\left.\begin{aligned} \left(\tfrac{1}{2}\mathbf{I} + \mathbf{H}_0 + \mathbf{P}_0 + \boldsymbol{n}^0 \mathbf{h}_0\right)\boldsymbol{v}^0 - \sum_{j=1}^{M} \left(\mathbf{H}_j + \boldsymbol{n}^0 \mathbf{h}_j\right)\boldsymbol{v}^j & \\ = \sum_{j=0}^{M} \left(\mathbf{G}_j + \boldsymbol{n}^0 \mathbf{g}_j\right)\boldsymbol{b}^j \quad (\boldsymbol{x} \in \Gamma_0) & \\ \left(\mathbf{H}_0 + \boldsymbol{n}^m \mathbf{h}_0\right)\boldsymbol{v}^0 - \sum_{j=1}^{M} \left(\mathbf{H}_j + \boldsymbol{n}^m \mathbf{h}_j\right)\boldsymbol{v}^j + \left(\tfrac{1}{2}\mathbf{I} + \mathbf{P}_m\right)\boldsymbol{v}^m & \\ = \sum_{j=0}^{M} \left(\mathbf{G}_j + \boldsymbol{n}^m \mathbf{g}_j\right)\boldsymbol{b}^j \quad (\boldsymbol{x} \in \Gamma_m). & \end{aligned}\right\} \tag{A 10}$$

In order to prove that the solution of (A 10) satisfies both the formulations (A 8) and (A 9), it is sufficient to show that the following equality is fulfilled:

$$w := \mathbf{g}_0 \boldsymbol{b}^0 - \mathbf{h}_0 \boldsymbol{v}^0 + \sum_{j=1}^{M} (\mathbf{g}_j \boldsymbol{b}^j + \mathbf{h}_j \boldsymbol{v}^j) = 0. \tag{A 11}$$

The validity of the latter equation can be shown by taking the inner product of (A 10) with respect to the outer normal, i.e. $\langle \boldsymbol{n}^m, \cdot \rangle_m$. In order to perform this we remark that

$$\langle \boldsymbol{n}^j, \mathbf{G}_m \boldsymbol{b}^m \rangle_j = \langle \mathbf{G}_j^* \boldsymbol{n}^j, \boldsymbol{b}^m \rangle_m = \langle \mathbf{G}_j \boldsymbol{n}^j, \boldsymbol{b}^m \rangle_m = 0, \tag{A 12}$$

which is deduced from the self-adjointness of $\mathbf{G}$ and (A 7). Note that we have only interchanged the integration variables. For the inner product of the rigid-body motions with respect to the outer normal, it can be shown that

$$\langle \boldsymbol{\varphi}^{mk}, \boldsymbol{n}^m \rangle_m = 0 \qquad (k = 1, 2, 3), \ (m = 0, .., M). \tag{A 13}$$

Now, we take the inner product of (A 10) with respect to the outer normal of $\Gamma_0$. Using (A 6), (A 12) and (A 13), it follows that

$$\begin{aligned} wL_0 &= \tfrac{1}{2}\langle \boldsymbol{n}^0, \boldsymbol{v}^0 \rangle_0 + \langle \boldsymbol{n}^0, \mathbf{H}_0 \boldsymbol{v}^0 \rangle_0 - \sum_{j=1}^{M} \langle \boldsymbol{n}^0, \mathbf{H}_j \boldsymbol{v}^j \rangle_0 \\ &= \tfrac{1}{2}\langle \boldsymbol{n}^0, \boldsymbol{v}^0 \rangle_0 + \langle \mathbf{H}_0^* \boldsymbol{n}^0, \boldsymbol{v}^0 \rangle_0 - \sum_{j=1}^{M} \langle \mathbf{H}_0^* \boldsymbol{n}^0, \boldsymbol{v}^j \rangle_j \\ &= \langle \boldsymbol{n}^0, \boldsymbol{v}^0 \rangle_0 - \sum_{j=1}^{M} \langle \boldsymbol{n}^j, \boldsymbol{v}^j \rangle_j, \end{aligned} \tag{A 14}$$

where $L_0$ is the curve length of the outer boundary $\Gamma_0$. Next, the inner product is taken of (A 10) with respect to the outer normal of $\Gamma_m$ $(m = 1, .., M)$, we obtain

$$\begin{aligned} wL_m &= \langle \boldsymbol{n}^m, \mathbf{H}_0 \boldsymbol{v}^0 \rangle_m - \sum_{j=1}^{M} \langle \boldsymbol{n}^m, \mathbf{H}_j \boldsymbol{v}^j \rangle_m + \tfrac{1}{2}\langle \boldsymbol{n}^m, \boldsymbol{v}^m \rangle_m \\ &= \langle \mathbf{H}_m^* \boldsymbol{n}^m, \boldsymbol{v}^0 \rangle_0 - \sum_{j=1}^{M} \langle \mathbf{H}_m^* \boldsymbol{n}^m, \boldsymbol{v}^j \rangle_j + \tfrac{1}{2}\langle \boldsymbol{n}^m, \boldsymbol{v}^m \rangle_m \\ &= -\tfrac{1}{2}\langle \boldsymbol{n}^m, \boldsymbol{v}^m \rangle_m + \tfrac{1}{2}\langle \boldsymbol{n}^m, \boldsymbol{v}^m \rangle_m = 0, \end{aligned} \tag{A 15}$$

where $L_m$ is defined analogously. From the latter equality it follows that $w$ has to be equal to zero; hence the solution of the deflated formulation (A 10) satisfies both the integrals (A 8) and (A 9). Furthermore, the inner product (A 14) reduces to the incompressibility requirement for the flow field.

## REFERENCES


Batchelor, G. K. 1967 *An Introduction to Fluid Dynamics.* Cambridge University Press.

Hopper, R. W. 1990 Plane Stokes flow driven by capillarity on a free surface. *J. Fluid Mech.* **213**, 349–375.

Hopper, R. W. 1991 Plane Stokes flow driven by capillarity on a free surface. Part 2. Further developments. *J. Fluid Mech.* **230**, 355–364.

Hopper, R. W. 1992 Stokes flow of a cylinder and half-space driven by capillarity. *J. Fluid Mech.* **243**, 171–181.

Hsiao, G. C. & Kress, R. 1985 On an integral equation for the two-dimensional exterior Stokes problem. *Appl. Numer. Math* **1**, 77–93.

Jagota, A. & Dawson, P. R. 1988*a* Micromechanical modeling of powder compacts-I. Unit problems for sintering and traction-induced deformation. *Acta. Metall.* **36**, 2551–2561.

Jagota, A. & Dawson, P. R. 1988*b* Micromechanical modeling of powder compacts-II. Truss formulation of discrete packings. *Acta. Metall.* **36**, 2563–2573.

JAGOTA, A. & DAWSON, P. R. 1990 Simulation of the viscous sintering of two particles. *J. Am. Ceram. Soc.* **73**, 173–177.

KIM, S. & KARRILA, S. J. 1991 *Microhydrodynamics: Principles and Selected Applications.* Butterworth-Heinemann.

KORWIN, D. M., LANGE, S. R., EATON, W. C., JOSEPH, I. & PYE, L. D. 1992 A study of the sintering behavior of glass in two geometric configurations. In *Proc. 16$^h$ Intl Congress on Glass*, published as a special issue of *Boletín de la Sociedad Española de Cerámica y Virdo.*

KUIKEN, H. K. 1990 Viscous sintering: the surface-tension-driven flow of a liquid form under the influence of curvature gradients at its surface. *J. Fluid Mech.* **214**, 503–515.

KREYSZIG, E. 1978 *Introductory Functional Analysis with Applications.* Wiley.

KRESS, R. 1989 *Linear Integral Equations.* Springer-Verlag.

LADYZHENSKAYA, O. A. 1963 *The Mathematical Theory of Viscous Incompressible Flow.* Gordon and Breach.

LORENTZ, H. A. 1896 Eene Algemeene Stelling omtrent de Beweging eener Vloeistof met Wrijving en eenige daaruit afgeleide Gevolgen. *Versl. Acad. Wetensch. Amsterdam* **5**, 168–175 (Transl. in *Collected Papers* **4**, pp. 7–14, Martinus Nijhoff (1937)).

POZRIKIDIS, C. 1992 *Boundary Integral and Singularity Methods for Linearized Viscous Flow.* Cambridge University Press.

RICHARDSON, S. 1992 Two-dimensional slow viscous flows with time-dependent free boundaries driven by surface tension. *Eur. J. Appl. Maths.* **3**, 193–207.

ROSS, J. W., MILLER, W. A. & WEATHERLY, G. C. 1981 Dynamic computer simulation of viscous flow sintering kinetics. *J. Appl. Phys.* **52**, 3884–3888.

SCHERER, G. W. 1984 Viscous sintering of a bimodal pore-size distribution. *J. Am. Ceram. Soc.* **67**, 709–715.

SŌMIYA, S. & MORIYOSHI, Y. (ed.) 1990 *Sintering Key Papers.* Elsevier.

TANZOSH, J., MANGA, M. & STONE, H. A. 1992 Boundary integral methods for viscous free-boundary problems: deformation of single and multiple fluid-fluid interfaces. In *Proc. Conf. on Boundary Element Technology VII* (ed. C. A. Brebbia & M. S. Ingber), pp. 19–39. Computational Mechanics Publications, Southampton.

VORST, G. A. L. VAN DE & MATTHEIJ, R. M. M. 1991 Implementing the boundary element method for 2-D viscous sintering. In *Proc. Conf. on Computational Modelling of Free and Moving Boundary Problems, Vol.1 Fluid Flow* (ed. L. C. Wrobel & C. A. Brebbia), pp. 341–355. Computational Mechanics Publications, Southampton.

VORST, G. A. L. VAN DE, MATTHEIJ, R. M. M. & KUIKEN, H. K. 1992 A boundary element solution for two-dimensional viscous sintering. *J. Comput. Phys.* **100**, 50–63.

VORST, G. A. L. VAN DE & MATTHEIJ, R. M. M. 1992*a* A BDF-BEM scheme for modelling viscous sintering. In *Proc. Conf. on Boundary Element Technology VII* (ed. C. A. Brebbia & M. S. Ingber), pp. 59–74. Computational Mechanics Publications, Southampton.

VORST, G. A. L. VAN DE & MATTHEIJ, R. M. M. 1992*b* Numerical analysis of a 2-D viscous sintering problem with non smooth boundaries. *Computing* **49**, 239–263.

WEINBAUM, S., GANATOS, P. & YAN, Z. Y. 1990 Numerical multipole and boundary integral equation techniques in Stokes flow. *Ann. Rev. Fluid Mech.* **22**, 275–316.